Organization of hippocampal CA3 into correlated cell assemblies supports a stable spatial code

Cell Reports

Article

Organization of hippocampal CA3 into correlated cell assemblies supports a stable spatial code

Graphical abstract

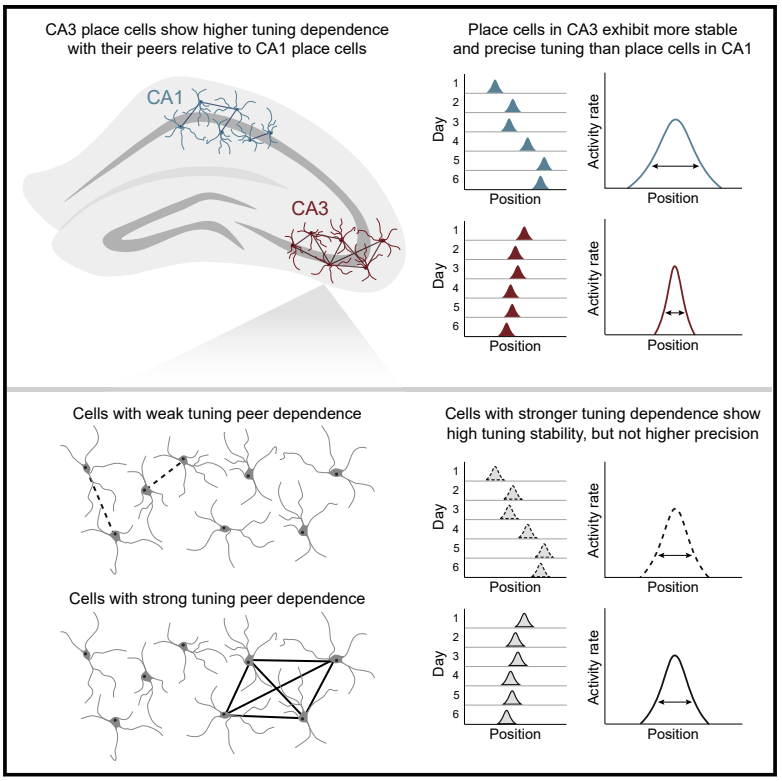

Highlights

- Ca^{2+} imaging allows studying place cells' precision, stability, and collective coding
- Place cells in CA3 exhibit more precise and stable tuning than place cells in CA1
- CA3 displays a collective organization into correlated place cell assemblies
- High correlations with cell peers underlie high tuning stability, but not precision

Authors

Liron Sheintuch, Nitzan Geva, Daniel Deitch, Alon Rubin, Yaniv Ziv

Correspondence

alon.rubin@weizmann.ac.il (A.R.), yaniv.ziv@weizmann.ac.il (Y.Z.)

In brief

Sheintuch et al. study the three-way relationship between precision, stability, and assembly organization of hippocampal place cells. Place cells in CA3 exhibit more precise and stable tuning than in CA1 and display a stronger cell assembly organization. The assembly organization contributes to stability, but not precision, of hippocampal spatial coding.

Sheintuch et al., 2023, Cell Reports *42*, 112119
February 28, 2023
https://doi.org/10.1016/j.celrep.2023.112119

CellPress

Cell Reports

CellPress
OPEN ACCESS

Article

Organization of hippocampal CA3 into correlated cell assemblies supports a stable spatial code

Liron Sheintuch,[1] Nitzan Geva,[1] Daniel Deitch,[1] Alon Rubin,[1,2,*] and Yaniv Ziv[1,2,3,*]
[1]Department of Brain Sciences, Weizmann Institute of Science, Rehovot, Israel
[2]These authors contributed equally
[3]Lead contact
*Correspondence: alon.rubin@weizmann.ac.il (A.R.), yaniv.ziv@weizmann.ac.il (Y.Z.)
https://doi.org/10.1016/j.celrep.2023.112119

SUMMARY

Hippocampal subfield CA3 is thought to stably store memories in assemblies of recurrently connected cells functioning as a collective. However, the collective hippocampal coding properties that are unique to CA3 and how such properties facilitate the stability or precision of the neural code remain unclear. Here, we performed large-scale Ca^{2+} imaging in hippocampal CA1 and CA3 of freely behaving mice that repeatedly explored the same, initially novel environments over weeks. CA3 place cells have more precise and more stable tuning and show a higher statistical dependence with their peers compared with CA1 place cells, uncovering a cell assembly organization in CA3. Surprisingly, although tuning precision and long-term stability are correlated, cells with stronger peer dependence exhibit higher stability but not higher precision. Overall, our results expose the three-way relationship between tuning precision, long-term stability, and peer dependence, suggesting that a cell assembly organization underlies long-term storage of information in the hippocampus.

INTRODUCTION

The hippocampus is known for its role in episodic and long-term memory and its contribution to spatial cognition.[1–5] From a theoretical point of view, the hippocampus has been postulated to function as a content-addressable memory system with auto-associative capabilities, allowing long-term storage of memories as stable attractor states.[6–10] These capabilities have been thought to originate in hippocampal subfield CA3 because of the abundance of recurrent excitatory synaptic connectivity between pyramidal cells within it.[11,12] This is in contrast to hippocampal CA1, where local connectivity is mostly between pyramidal cells and interneurons,[13] making it less suited for supporting such auto-associative capabilities. The number of stable attractor states that can be stored by an auto-associative network depends on the fraction of cells that participate in the representation of each item (e.g., a given position within an environment).[7,8,14,15] Thus, more localized (precise) tuning curves are predicted to correspond to a higher stability of the stored set of network states. Consistent with the hippocampal circuit architecture and the hypothesized role of CA3 in long-term storage of memories, experimental studies have found more precise[16] and more stable[17–20] representations in CA3 than in CA1. However, it remains unclear whether cooperation between large populations of pyramidal cells within the hippocampus is a unique feature of CA3 and whether such cooperation serves as a neuronal mechanism underlying the precision and stability of the hippocampal code.

Recent advances in optical imaging techniques allow chronic readout of activity from hundreds of simultaneously recorded neurons in freely behaving mice[21–23] and to reliably follow the same cells across multiple weeks.[24] Therefore, such techniques enable studying the collective coding properties of hippocampal CA3 neurons and how such properties could support the stable storage and retrieval of information over long timescales. Capitalizing on the advantages of Ca^{2+} imaging techniques, we longitudinally recorded from large populations of CA1 and CA3 neurons in mice that repeatedly explored the same environments over weeks and compared the collective coding properties across these two hippocampal subfields. We found that CA3 is organized into assemblies of functionally correlated cells and that this organization contributes to the long-term stability, but not to the precision, of the hippocampal spatial code.

RESULTS

Establishing a preparation for chronic Ca^{2+} imaging in hippocampal CA3 of freely behaving mice

To compare the collective coding properties of CA1 and CA3, we sought to chronically image large populations of pyramidal neurons expressing the Ca^{2+} indicator GCaMP6f in each of these two hippocampal subfields. Performing Ca^{2+} imaging of the dorsal CA1 of freely behaving mice has become a relatively standard procedure.[21,25–27] However, imaging of CA3 is more challenging because of its less accessible location within the hippocampus. To optically access CA3 neurons without damaging the rest of the hippocampus, we implanted a microendoscope equipped with a micro-prism anterior to the hippocampus[28] (Figure 1A). We verified the location of the micro-prism implantation

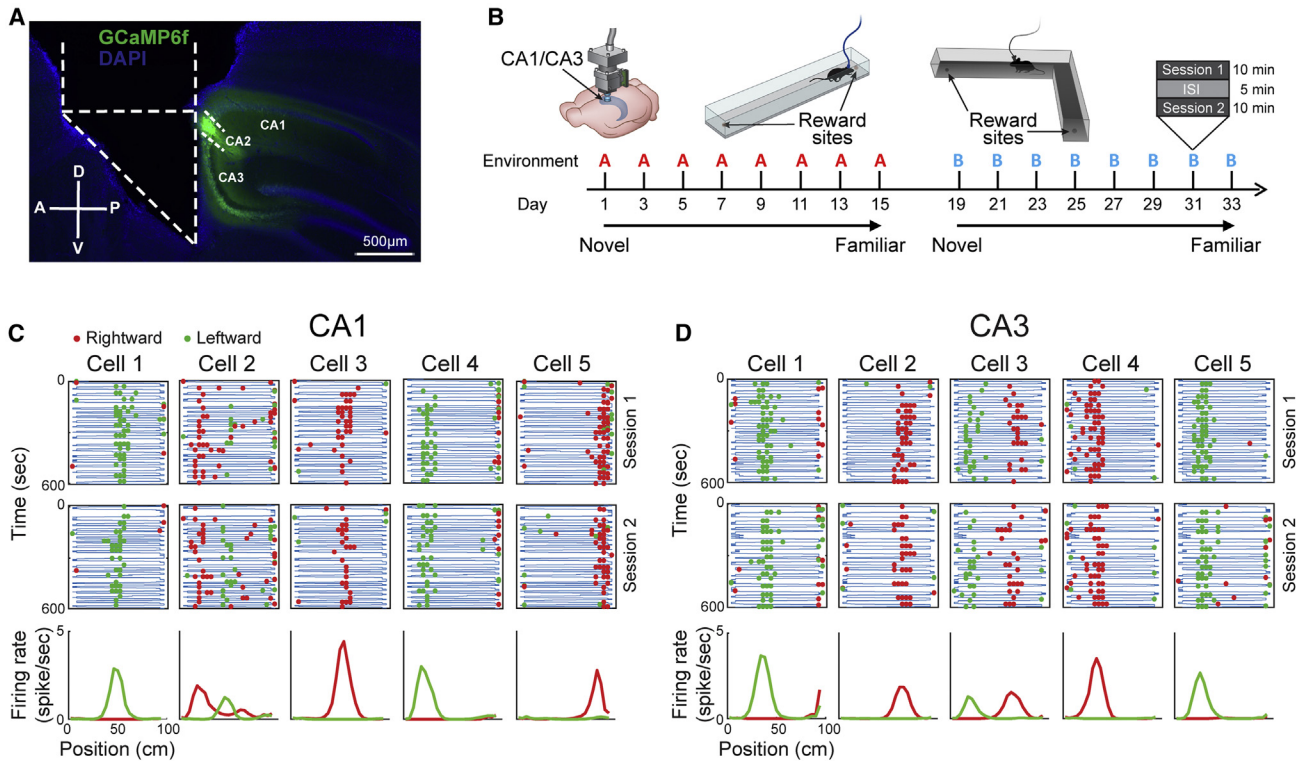

Figure 1. Ca^{2+} imaging of hippocampal CA1 and CA3 of freely behaving mice during familiarization with novel environments over weeks

(A) Representative example of a sagittal section of a mouse implanted with a micro-prism anterior to the hippocampal CA3, showing GCaMP6f expression (green) and DAPI-labeled cell nuclei (blue). The micro-prism location is shown in white. Scale bar, 500 μm. D, dorsal; V, ventral; A, anterior; P, posterior.

(B) Ca^{2+} imaging in CA1 or in CA3 during free exploration of initially novel environments (straight and L-shaped linear tracks) every other day. The mice explored environment A on 8 imaging days and then environment B on the following 8 days. Each imaging day consisted of two 10-min sessions separated by a 5-min inter-session interval.

(C and D) Five example place cells recorded simultaneously from a mouse imaged in CA1 (C) and a mouse imaged in CA3 (D). Top: position of the mouse at times of estimated neuronal spikes (red and green dots for rightward and leftward running directions, respectively) overlaid on the mouse trajectory (blue curve). Bottom: corresponding spatial tuning curves, shown separately for rightward (red) and leftward (green) running directions.

postmortem by immunohistochemistry labeling of the adjacent CA2 using PCP4 (Figure S1A).

We performed Ca^{2+} imaging every other day from pyramidal cells in either CA1 (n = 4 mice) or CA3 (n = 5 mice) while the mice freely explored two different, initially novel linear track environments (Figure 1B). During the first 8 imaging days, the mice explored environment A, and then, for 8 additional imaging days, they explored environment B. This experimental design allowed us to study the formation and long-term stability of hippocampal spatial representations during familiarization and to examine whether collective coding properties are shared across two different spatial contexts. Each imaging day consisted of two consecutive 10-min sessions separated by a 5-min inter-session interval. We used previously established routines[29] to detect separated Ca^{2+} sources corresponding to individual cells and estimate their underlying spike trains from the imaging data (Figures S1B–S1F). This procedure yielded comparable numbers of cells between CA1 and CA3 (465 ± 147 versus 334 ± 190 detected cells in CA1 and CA3, respectively) and similar estimated firing rates (0.22 ± 0.07 versus 0.19 ± 0.11 spikes/s in CA1 and CA3, respectively; Figures S1G and S1H). The number of track traversals per day was also similar between the two groups of mice (66.6 ± 8.7 versus 57.2 ± 20.4 traversals per day in CA1 and CA3, respectively; Figure S1I). In agreement with previous studies on hippocampal place cells,[4,30–33] a large fraction of CA1 and CA3 cells were tuned to mouse position while running in the track (50.5% ± 7.8% versus 42.8% ± 11.2% place cells of the active population in CA1 and CA3, respectively) and typically maintained their spatial tuning across the two different sessions within the same day while changing their tuning across the two running directions (Figures 1C and 1D).

CA3 place cells are more precisely tuned to position in novel environments than CA1 place cells

First, we studied the spatial tuning precision of individual hippocampal neurons by calculating the spatial information carried by the activity of place cells. Because naive estimation of information from limited sample sizes suffers from an upward bias,[34] we estimated information content using bias correction methods we recently developed that are specifically tailored for the temporally sparse neuronal activity obtained from Ca^{2+} imaging data.[35] We found that place cells in CA3 carried significantly

higher spatial information than place cells in CA1 in the first 3 imaging days in each environment (1.21 ± 0.09 versus 1.48 ± 0.14 bit/spike in CA1 and CA3, respectively; Figures 2A and 2B). The higher spatial information carried by place cells in CA3 was not explained by smaller place field sizes (Figure S2A) but rather by a smaller number of place fields per cell (Figure S2B). Moreover, we found that spatial information content in CA1 and CA3 place cells increased over the course of familiarization with the environment (Figure 2C), validating previous reports of hippocampal coding precision gradually increasing during learning.[32,36,37] Interestingly, the increase in information over time was greater in CA1, gradually closing the gap on CA3 as the mice became familiar with the environments. Next, we measured the similarity in the activity of all place cells across different positions and running directions by calculating the population vector (PV) correlations between each pair of positions and across both running directions in the track (Figures 2D and 2E). CA1 and CA3 place cells were highly specific to the running direction in the track, exhibiting comparable near-zero PV correlations between the representations of the same position in the two running directions (0.04 ± 0.02 versus 0.07 ± 0.05 PV correlation in CA1 and CA3, respectively; Figure 2F), in agreement with previous reports of global remapping across directions.[33,38–40] The spatial code similarity across directions was higher in one environment (an L-shaped track) than in the other environment (a straight linear track) in CA1 but not in CA3 (Figure 2G, inset), suggesting that the corner in the L-shaped track serves as a salient visual cue promoting a view-invariant spatial representation in CA1.[40] The spatial code similarity across running directions decreased over time in both hippocampal subfields as the environments became familiar (Figure 2G), suggesting that the hippocampus actively separates the representations of the two directions.[41] We also measured the short-term stability of the spatial representations by calculating the PV correlations between the representations of the same position and running direction across the pairs of consecutive sessions imaged 5 min apart. This analysis revealed higher short-term stability in CA3 than in CA1 in the first three imaging days in each environment (0.62 ± 0.03 versus 0.78 ± 0.04 PV correlation across sessions in CA1 and CA3, respectively; Figure 2H). Similar to tuning precision, the short-term stability of the spatial representations increased over time[42] in both hippocampal subfields but to a greater extent in CA1 (Figure 2I). These results are in line with the role of CA3 in rapid one-trial contextual learning[20,32,43,44] and suggest that CA1 may inherit its tuning properties from CA3 throughout the process of familiarization. The dynamics of the improvement in most aspects of the hippocampal spatial code during learning did not differ across the two environments (Figures S2C–S2E). We also recapitulated the changes in the spatial tuning properties over time while subsampling the data to obtain a fixed number of track traversals across days and mice, verifying that our results are not due to changes in animal behavior that occur with learning (Figures S2F–S2I). Overall, we demonstrated that, in novel environments, CA3 place cells exhibit higher tuning precision and short-term stability than CA1 place cells, while the spatial representations in CA1 undergo a higher degree of refinement throughout the process of familiarization.

CA3 spatial representations are more stable over weeks than CA1 spatial representations

Taking advantage of the ability to reliably track the same populations of neurons over weeks with Ca^{2+} imaging,[21,24] we next studied the long-term stability of the hippocampal spatial representations. We registered the cells across all imaging days, which yielded similar numbers of registered cells (1,070 ± 272 versus 817 ± 317 registered cells per mouse for CA1 and CA3, respectively) and comparable registration accuracy (7.6% ± 0.8% versus 12.0% ± 4.1% estimated registration error rates for CA1 and CA3, respectively; Figures S3A–S3G). Then, we calculated the neuronal ensemble rate correlations across days, which measure the similarity in the cells' activity levels throughout the entire session irrespective of position (Figure 3A). The ensemble rate correlations as a function of the time difference between pairs of sessions were comparable between CA1 and CA3 (Figure 3B). However, the long-term stability of the spatial representations, as quantified by the PV correlations across days and weeks, was significantly higher in CA3 than in CA1 (Figures 3C and 3D), in agreement with previous studies.[17–20] Similar results were obtained while controlling for differences in the overall number of registered cells across mice and hippocampal subfields (Figures S3H and S3I). Together, our results demonstrate that hippocampal CA3 can support the stable maintenance of spatially precise representations over long timescales.

Hippocampal CA3 is organized into functionally related place cell assemblies

To study the emergent collective coding properties within the hippocampus, we looked for a statistical dependence between place cells that could not be explained by the spatial tuning properties of individual cells (Figure 4A, illustration). To this end, we calculated the distribution of pairwise tuning-curve correlations across all the recorded cells that were tuned to position in a given running direction. While the distributions seemed similar, a significantly larger fraction of cell pairs in CA3 had high tuning-curve correlations (3.0% ± 0.2% versus 4.8% ± 0.9% of cell pairs with a correlation > 0.7 for CA1 and CA3, respectively; Figure 4B). Next, we focused on the more correlated pairs of cells and asked whether place cells with the same preferred position exhibit a similarity between the shapes of their tuning curves (Figure 4C, illustration). We found that the tuning-curve correlations between pairs of place cells with the same preferred position were considerably higher in CA3 than in CA1 (40.0% ± 2.2% versus 54.9% ± 6.8% of cell pairs with a correlation > 0.7 for CA1 and CA3, respectively; Figure 4D). However, because pairwise tuning-curve correlations and spatial information are correlated (Figure S4A), the higher pairwise tuning correlations in CA3 could also stem from the higher tuning precision in this hippocampal subfield and not necessarily from a dependence between cells. To address this issue, instead of directly comparing the correlations in CA1 with those in CA3, we sought to compare the correlations in each mouse against the correlations obtained from a set of cells with matching tuning precision and pairwise tuning correlations but with independent tuning curves (Figure 4E, illustration). Because the spatial tuning of place cells randomly remaps across running directions in the linear track

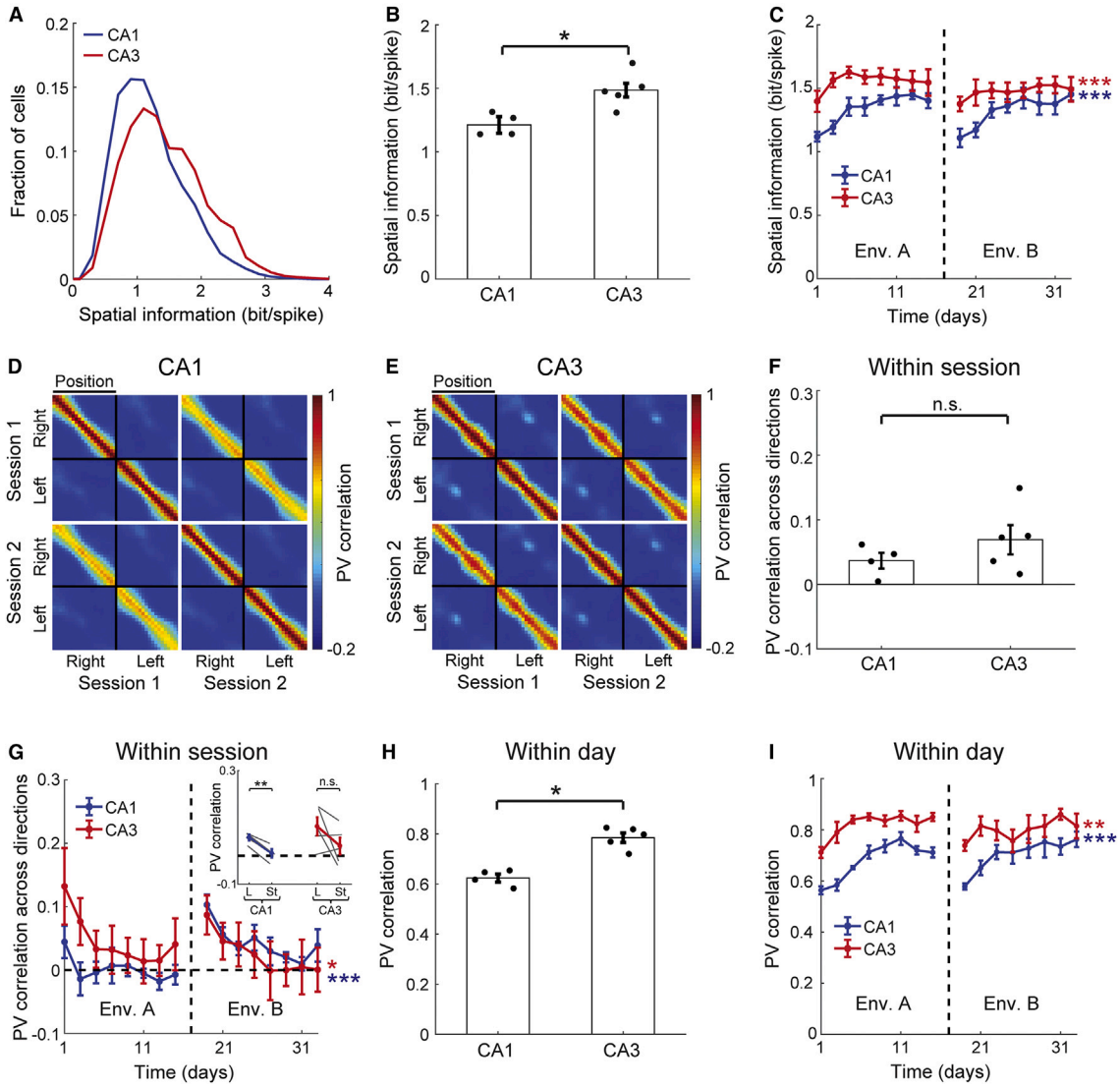

Figure 2. CA3 place cells exhibit higher spatial tuning precision and short-term stability than CA1 place cells

(A) Distributions of average spatial information content carried by the activity of individual hippocampal place cells on the first 3 imaging days in each environment in CA1 (blue) and in CA3 (red).

(B) Spatial information of place cells on the first 3 imaging days in each environment (mean ± SEM) was significantly higher in CA3 than in CA1 (Mann-Whitney U test, $U = 11$, $p < 0.05$).

(C) Spatial information (mean ± SEM) increased over the days of the experiment in CA1 (blue; one-way repeated-measures ANOVA, $F_{(15)} = 6.51$, $p < 10^{-6}$) and CA3 (red; one-way repeated-measures ANOVA, $F_{(15)} = 3.74$, $p < 0.001$). The increase in information over time was greater in CA1 than in CA3 (two-way repeated-measures ANOVA, $F_{(1,15)} = 2.56$, $p < 0.01$, interaction between hippocampal subfield and time).

(D and E) PV correlation between all pairs of positions across the two running directions for CA1 (D) and CA3 (E). The correlations were averaged across the first 3 imaging days in each environment and over mice.

(F) PV correlation between the same positions across the opposite running directions in the track on the first 3 imaging days in each environment (mean ± SEM) was not significantly different between CA1 and CA3 (Mann-Whitney U test, $U = 15$, $p = 0.29$).

(G) PV correlation between the same positions across the opposite running directions (mean ± SEM) decreased over the days of the experiment for CA1 (blue; one-way repeated-measures ANOVA, $F_{(15)} = 4.81$, $p < 10^{-4}$) and CA3 (red; one-way repeated-measures ANOVA, $F_{(15)} = 2.05$, $p < 0.05$). Inset: the across-directions PV correlations on the first 3 imaging days in each environment were significantly higher in the L-shaped than in the straight linear track in CA1 (matched-pairs t test, $t_{(3)} = 7.82$, $p < 0.01$) but not in CA3 (matched-pairs t test, $t_{(4)} = 1.70$, $p = 0.16$).

(H) PV correlation between the pairs of sessions imaged 5 min apart on the first 3 imaging days in each environment (mean ± SEM) was significantly higher in CA3 than in CA1 (Mann-Whitney U test, $U = 10$, $p < 0.05$).

(I) PV correlation between pairs of sessions imaged 5 min apart (mean ± SEM) increased over the days of the experiment for CA1 (blue; one-way repeated-measures ANOVA, $F_{(15)} = 7.11$, $p < 10^{-6}$) and CA3 (red; one-way repeated-measures ANOVA, $F_{(15)} = 2.75$, $p < 0.01$). CA1 exhibited a greater increase in PV correlations over time (two-way repeated-measures ANOVA, $F_{(1,15)} = 1.81$, $p < 0.05$, interaction between hippocampal subfield and time).

Data were averaged over 4 mice in CA1 and 5 mice in CA3. *$p < 0.05$, **$p < 0.01$, ***$p < 0.001$.

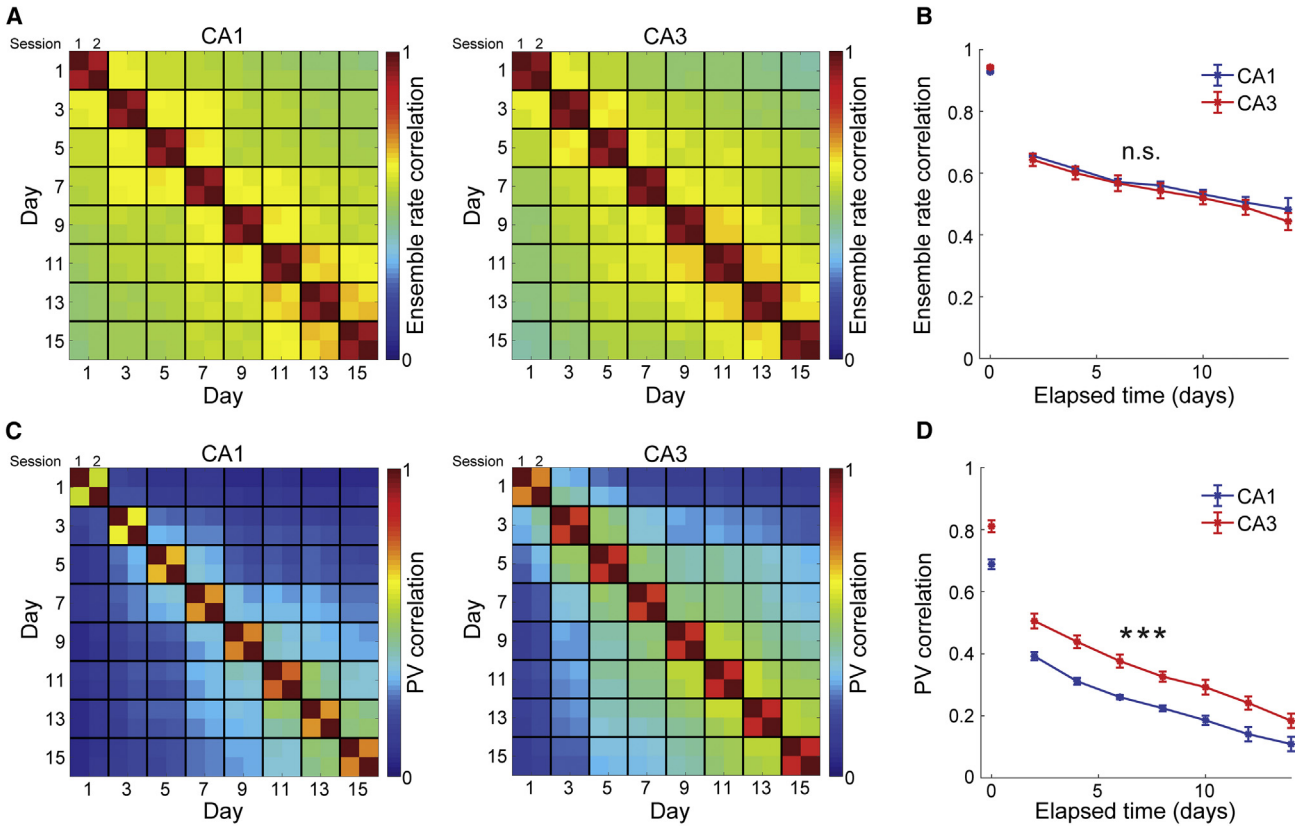

Figure 3. CA3 exhibits more stable spatial representations over weeks than CA1

(A) Average ensemble rate correlations of place cells across all sessions in the same environment for CA1 (left) and CA3 (right). Correlations were averaged over the two environments and all mice.

(B) Ensemble rate correlation of place cells between pairs of sessions as a function of elapsed time between them (mean ± SEM) was not significantly different between CA1 (blue) and CA3 (red; two-way repeated-measures ANOVA, $F_{(1,7)} = 0.29$, $p = 0.61$, main effect of hippocampal subfield).

(C) Average PV correlations of place cells across all sessions in the same environment for CA1 (left) and CA3 (right). Correlations were averaged over the two environments and all mice.

(D) PV correlation between pairs of sessions as a function of elapsed time between them (mean ± SEM) was significantly higher in CA3 (red) than in CA1 (blue; two-way repeated-measures ANOVA, $F_{(1,7)} = 29.7$, $p < 0.001$, main effect of hippocampal subfield).

Data were averaged over 4 mice in CA1 and 5 mice in CA3. ***$p < 0.001$.

(Figures 2D–2G), cells from the same mouse that are tuned to the opposite running direction meet all of these criteria (Figures S4B and S4C). Therefore, we compared in each mouse the distribution of tuning correlations across pairs of cells with the same preferred position in a given running direction against a null distribution obtained between pairs of cells tuned to the same position but across the opposite running directions (Figure 4F). The difference between the within-direction and across-directions distributions was significantly higher in CA3 than in CA1 (Figure 4G). As an additional validation of this effect, we compared the distributions of pairwise tuning correlations within a given mouse with those obtained across place cells from different mice imaged in the same hippocampal subfield, which yielded similar results (Figures S4D and S4E). These findings point to an emergent collective assembly organization in hippocampal CA3, wherein the tuning of place cells shows a higher statistical dependence with their peers. Similar results were also obtained when excluding pairs of cells that were less than 50 μm apart within the brain tissue (Figure S4F), confirming that the stronger assembly organization observed in CA3 is not due to higher cross-talk between the Ca^{2+} signals of neighboring cells. We did not find any sign that the collective assembly organization was shared across the two different spatial contexts, possibly because of the global remapping observed across sessions in the different environments (Figures S4G–S4I). Next, we assessed whether the assembly organization is specific to functionally related place cells by also calculating the distributions of pairwise tuning correlations between cells with different preferred positions. Indeed, the statistical dependence of place cells on their peers decreased with the difference between their preferred positions (Figures 4H and 4I). Finally, we compared the temporal organization of the activity patterns of CA3 and CA1 place cells by calculating the pairwise noise correlations. Consistent with our finding of a collective organization of the spatial tuning curves, pairs of place cells in CA3 with the same preferred position had higher noise correlations than such cell

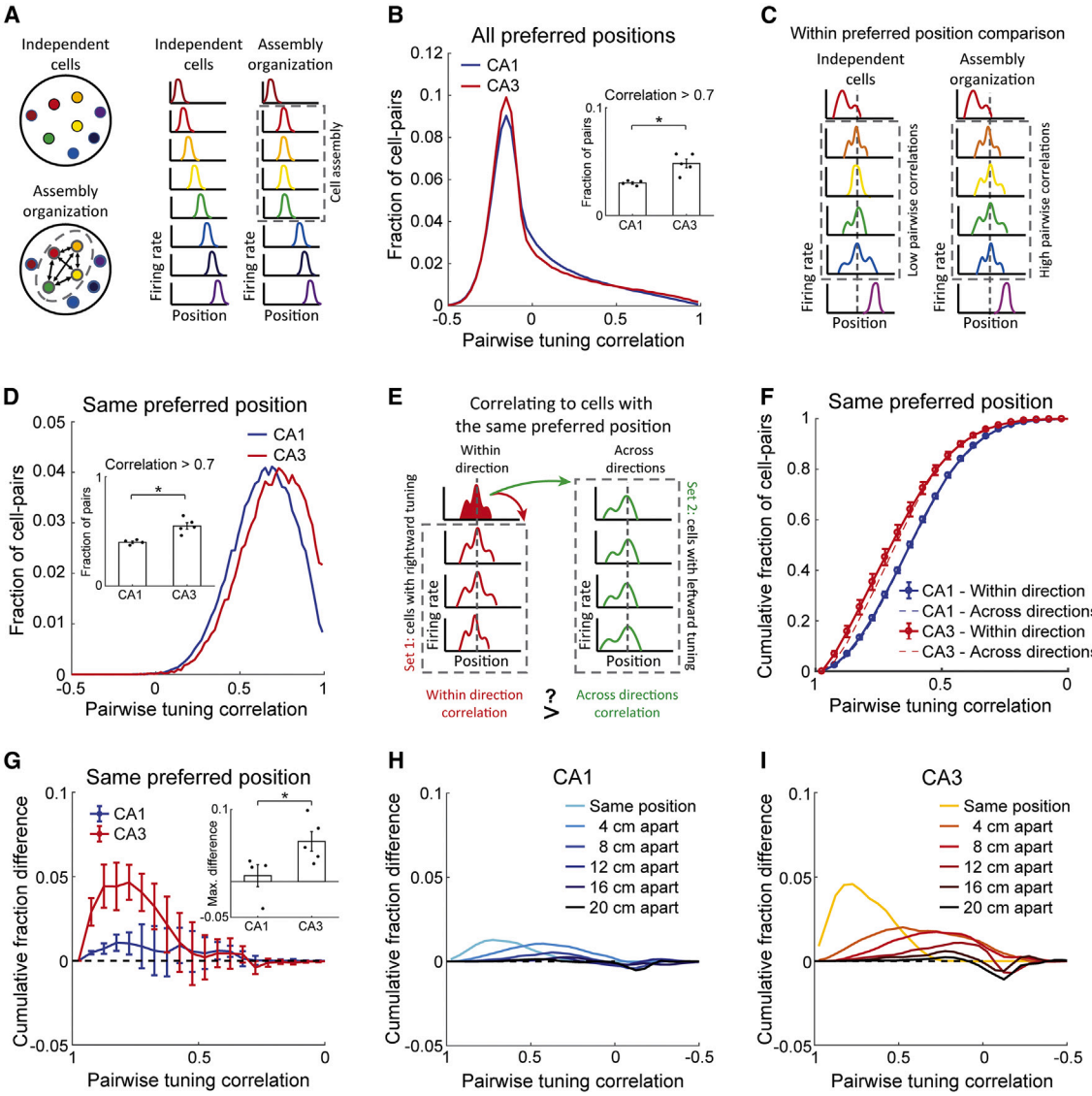

Figure 4. Hippocampal CA3 is organized into functionally related place cell assemblies

(A) Illustration of a population of place cells with independent tuning curves versus tuning curves of cells that are organized into a cell assembly.

(B) Distribution of pairwise tuning-curve correlations for all pairs of place cells for CA1 (blue) and CA3 (red). Inset: the fraction of cell pairs with a tuning correlation greater than 0.7 was significantly higher in CA3 than in CA1 (Mann-Whitney U test, $U = 10$, $p < 0.05$).

(C) Illustration of a population of place cells that have the same preferred position with independent shapes of their tuning curves (left) versus a population that is organized into a cell assembly with similar shapes of their tuning curves (right).

(D) Distribution of pairwise tuning-curve correlations across all pairs of place cells with the same preferred position for CA1 (blue) and CA3 (red). Inset: fraction of cell pairs with the same preferred position with a tuning correlation greater than 0.7 was significantly higher in CA3 than in CA1 (Mann-Whitney U test, $U = 10$, $p < 0.05$).

(E) Illustration of a population of place cells that have the same preferred position in either the rightward or leftward running direction. If place cells exhibit a dependence between the shapes of their tuning curves, then the tuning correlations between cells with the same preferred position in the same running direction are expected to be higher than the correlations between pairs of cells with the same preferred position across the opposite running directions.

(F) Cumulative distributions of pairwise tuning-curve correlations between cell pairs with the same preferred position (mean ± SEM) for CA1 (blue) and CA3 (red). The within-running-direction distributions (solid curves) are shown against the across-running-direction distributions (dashed curves).

(G) Difference between the cumulative within-running-direction and across-running-directions distributions of pairwise tuning-curve correlations (mean ± SEM) for CA1 (blue) and CA3 (red). Inset: the maximal difference between the cumulative distributions was significantly higher in CA3 than in CA1 (Mann-Whitney U test, $U = 11$, $p < 0.05$).

(H and I) Difference between the cumulative within-running-direction and across-running-direction distributions of pairwise tuning-curve correlations (mean) across all pairs of place cells with the same or with different preferred positions for CA1 (H) and CA3 (I).

Note that the x axis in (F)–(I) goes from the high correlations to the low correlations. Data were averaged across the first 3 imaging days in each environment. Data were averaged over 4 mice in CA1 and 5 mice in CA3. *$p < 0.05$.

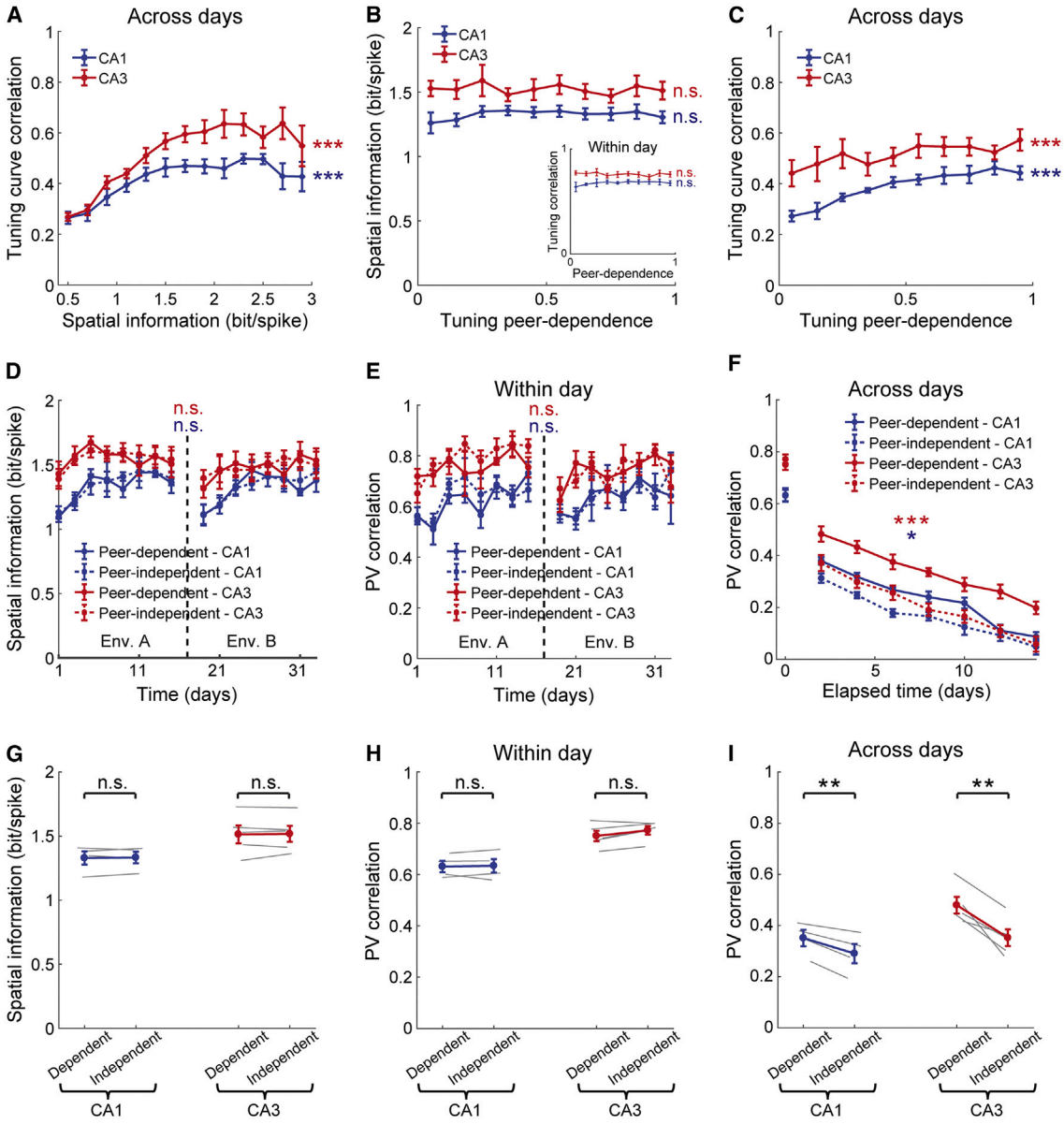

Figure 5. Place cells with peer-dependent tuning exhibit higher long-term tuning stability but not higher tuning precision

(A–C) Relationship between long-term tuning stability, tuning precision, and tuning peer dependence at the single-cell level.

(A) Tuning-curve correlations between sessions imaged 2 days apart increase as a function of the spatial information (mean ± SEM) in CA1 (blue; multiple regression $t = 22.4$, $p < 10^{-100}$) and CA3 (red; multiple regression $t = 19.1$, $p < 10^{-79}$).

(B) Spatial information does not change with the level of tuning peer dependence (mean ± SEM) in CA1 (blue; multiple regression $t = 0.38$, $p = 0.70$) or CA3 (red; multiple regression $t = 1.82$, $p = 0.07$). Inset: tuning-curve correlation between sessions imaged 5 min apart does not change with the level of tuning peer dependence (mean ± SEM) in CA1 (blue; multiple regression $t = -0.07$, $p = 0.94$) or CA3 (red; multiple regression $t = -1.70$, $p = 0.09$).

(C) Tuning-curve correlations between sessions imaged 2 days apart increase as a function of the level of tuning peer dependence (mean ± SEM) in CA1 (blue; multiple regression $t = 12.0$, $p < 10^{-32}$) and CA3 (red; multiple regression $t = 8.8$, $p < 10^{-17}$).

(A–C) A linear multiple regression model was separately fitted to the data of each hippocampal subfield between the tuning-curve correlation, spatial information, tuning peer dependence, average estimated firing rate, and mouse identity of each cell.

(D–I) Comparison of the precision and stability of spatial tuning between place cells that were highly correlated with their peers (peer-dependent cells) and place cells that were not (peer-independent cells).

(D) Spatial information over the days of the experiment (mean ± SEM) did not differ between the peer-dependent (solid) and peer-independent (dashed) cells in CA1 (blue; Friedman's test, $\chi^2_{(1)} = 0.13$, $p = 0.72$) or CA3 (red; Friedman's test, $\chi^2_{(1)} = 0.39$, $p = 0.53$).

(E) PV correlation between two sessions imaged 5 min apart over the days of the experiment (mean ± SEM) was not different between the peer-dependent cells (solid) and the peer-independent cells (dashed) in CA1 (blue; Friedman's test, $\chi^2_{(1)} = 0.08$, $p = 0.77$) or CA3 (red; Friedman's test, $\chi^2_{(1)} = 1.51$, $p = 0.22$).

(legend continued on next page)

pairs in CA1 (Figure S4J). We also found that noise correlations between pairs of place cells decreased as a function of the difference in their preferred position (Figure S4K) or as a function of the distance between them in the brain tissue (Figure S4L). Overall, our results uncover an emergent collective assembly organization of hippocampal CA3 place cells that goes beyond the tuning properties of individual neurons.

Place cells with stronger tuning peer dependence exhibit higher long-term tuning stability but not higher tuning precision

Finally, we sought to study the contribution of the organization of CA3 into place cell assemblies to the precision and stability of the hippocampal spatial code. To this end, we estimated for each cell the statistical dependence between its tuning and the tuning of its peers (tuning peer dependence). Specifically, for each cell, we found the median of its within-direction pairwise tuning correlations and then calculated into which percentile it falls within the distribution of its across-directions tuning correlations. The average percentile was greater than expected from a null hypothesis (50%) in CA1 and CA3 (51.1% ± 0.5%, t test, $t_{(3)} = 5.12$, $p < 0.05$, and 52.5% ± 1.3%, t test, $t_{(4)} = 4.31$, $p < 0.05$ for CA1 and CA3, respectively), further confirming the existence of a significant assembly organization. Then, we performed a multivariate regression analysis at the single-cell level between tuning stability, tuning precession, and tuning peer dependence (Figures 5A–5C). Because tuning precision and stability may also depend on the activity levels of the cells[45] (Figures S5A–S5C), the multivariate regression analysis also accounted for the average firing rate of each cell. The tuning-curve correlations across days for individual place cells were highly correlated with their spatial information content (Figure 5A), suggesting that tuning precision and long-term stability are linked. Surprisingly, while spatial information and within-day tuning-curve correlation did not change with the level of tuning peer dependence (Figure 5B), the tuning-curve correlation across days significantly increased as a function of the tuning peer dependence of individual place cells in both hippocampal subfields (Figure 5C). These differences between tuning precision and long-term stability with respect to their link to tuning peer dependence demonstrate a dissociation between these two seemingly related aspects of the hippocampal spatial code. Next, we divided the population of place cells into those that are highly correlated with their peers (peer-dependent cells; STAR Methods) and those that are not (peer-independent cells). We did not find differences in the spatial information (Figures 5D and 5G) or in the place field size (Figure S5D) between the peer-dependent and peer-independent cells in CA1 or CA3. Peer-dependent cells in CA3, but not in CA1, exhibited slightly more place fields per cell than the peer-independent cells (Figure S5E). Additionally, we did not find differences in short-term stability between the peer-dependent and peer-independent cells, as quantified by the PV correlations across the two consecutive sessions imaged 5 min apart (Figures 5E and 5H). Importantly, the peer-dependent cells in both hippocampal subfields displayed significantly higher long-term stability than the peer-independent cells, as quantified by the PV correlations across sessions from different days (Figures 5F and 5I). The ensemble rate correlations across days were also higher in the peer-dependent cells than in the peer-independent cells (Figure S5F), demonstrating that the higher long-term stability of these cells was also due to the higher conservation of their overall estimated firing rates and not only due to the higher spatial tuning stability. The noise correlations between pairs of cells with the same preferred position were higher for the peer-dependent cells than for the peer-independent cells in CA1 and CA3 (Figure S5G), suggesting that the temporal co-firing of cells may underlie the assembly organization of the spatial tuning curves. We did not find a difference in the average estimated firing rates between these two groups of cells that might underlie the differences we found in the long-term stability or pairwise noise correlations (Figure S5H). However, we did find that, in CA1, but not in CA3, the divergence of the distribution of preferred positions from a uniform distribution was higher for the peer-dependent cells compared with the peer-independent cells (Figure S5I). This result indicates that the higher long-term stability of peer-dependent cells in CA3 was not due to a tendency of these cells to represent specific landmarks, while in CA1, the increased stability of these cells may be mediated by an over-representation of landmarks. Taken together, our results suggest that the organization of CA3 into correlated place cell assemblies contributes to the long-term stability, but not to the tuning precision or short-term stability, of the hippocampal spatial code.

DISCUSSION

We established a preparation for chronic Ca^{2+} imaging in hippocampal CA3 of freely behaving mice and followed the activity of hundreds of simultaneously recorded neurons over days and weeks. This imaging preparation allowed us to compare the spatial coding properties of the recorded population between CA3 and CA1, revealing several differences between these two hippocampal subfields at the level of the tuning of individual neurons and at the level of the emergent collective coding behavior.

(F) PV correlation between pairs of sessions as a function of elapsed time between them (mean ± SEM) was significantly higher for the peer-dependent cells (solid) than for the peer-independent cells (dashed) in CA1 (blue; Friedman's test, $\chi^2_{(1)} = 6.51$, $p < 0.05$) and CA3 (red; Friedman's test, $\chi^2_{(1)} = 17.72$, $p < 10^{-4}$).
(G) Average spatial information across all imaging days (mean ± SEM) did not differ between the peer-dependent and peer-independent cells in CA1 (matched pairs t test, $t_{(3)} = -0.33$, $p = 0.76$) or CA3 (matched pairs t test, $t_{(4)} = -0.26$, $p = 0.81$).
(H) PV correlation (mean ± SEM) between sessions imaged 5 min apart did not differ between the peer-dependent and peer-independent cells in CA1 (matched pairs t test, $t_{(3)} = -0.32$, $p = 0.77$) or CA3 (matched pairs t test, $t_{(4)} = -2.36$, $p = 0.08$).
(I) PV correlation (mean ± SEM) between sessions imaged 2 days apart was significantly higher for the peer-dependent cells than for the peer-independent cells in CA1 (matched pairs t test, $t_{(3)} = 7.06$, $p < 0.01$) and CA3 (matched pairs t test, $t_{(4)} = 5.27$, $p < 0.01$).
(E, F, H, and I) Subsets of peer-independent cells were randomly chosen to match the peer-dependent cells' population size.
Data were averaged over 4 mice in CA1 and 5 mice in CA3. *$p < 0.05$, **$p < 0.01$, ***$p < 0.001$.

In agreement with previous electrophysiological studies, we found that CA3 neurons exhibit higher spatial tuning precision than CA1 neurons.[16] Moreover, we demonstrated that spatial representations in CA3 are more stable than those in CA1 over weeks, expanding previous work that compared the stability of the spatial code between CA1 and CA3 over shorter timescales of up to 2 days.[17–20] Together, these results show that CA3 can support precise and stable maintenance of spatial representations over long timescales.

The analysis of the activity of large populations of simultaneously recorded neurons allowed us to expose emergent collective coding properties in CA3 that are in line with the abundant recurrent excitatory connectivity in this hippocampal subfield[11,12] and with its hypothesized auto-associative capabilities.[6–10] Specifically, pairs of CA3 place cells that were tuned to similar positions in the environment displayed higher tuning-curve correlations than the correlations between independent cells with matching spatial tuning properties, a result that was significantly less pronounced in CA1. In addition, the noise correlations between pairs of cells with the same preferred position were higher in CA3 than in CA1. Earlier work demonstrated the pattern separation and pattern completion capabilities of hippocampal CA3,[30,46–53] two opposing computational outcomes characteristic of auto-associative networks. Our finding that CA3 place cells are organized into functionally related assemblies instead of operating as a set of cells that independently represent the environment[7] provides additional evidence of emergent collective computational capabilities in this hippocampal subfield.

Notably, we found that pairs of place cells in hippocampal CA1 display noise correlations greater than those expected by conditionally independent cells, in line with previous findings of collective computational capabilities in CA1.[54–61] Most previous studies of collective hippocampal coding properties focused only on CA1, the downstream target of CA3, which is easier to experimentally access and record from. The emphasis on CA1 led to a conceptual gap between anatomically and theoretically based predictions of finding collective coding properties in CA3 and neurophysiological experiments demonstrating collective coding in CA1. The observed collective coding properties in CA1 were typically interpreted as reflecting network dynamics in CA3, but the difference in the degree of collective coding between the two hippocampal subfields was not directly tested. Our demonstration of a stronger assembly organization in CA3 than in CA1 experimentally reconciles this long-standing conceptual gap.

Our finding that CA3 exhibits a pronounced assembly organization in a novel environment is consistent with the observation of preplays and the notion that the hippocampus can represent new spatial experiences by selecting from a repertoire of preconfigured network states.[62–64] Notably, the assembly organization was not conserved across the two different environments, suggesting that collective coding in the hippocampus is flexible and subjected to minimal interference between different memories. Studying hippocampal collective coding using techniques with higher temporal resolution, such as dense electrophysiology, could help further elucidate how the assembly organization we observed is related to hippocampal replays or fast theta sequences.[65–69]

Importantly, we found in CA1 and in CA3 that place cells with stronger tuning peer dependence had considerably more stable spatial tuning over long time periods, maintaining their spatial preference and their average firing rate. Yet, tuning peer dependence did not seem to underlie higher tuning precision or short-term stability. These results are surprising because tuning precision and long-term tuning stability were highly correlated across cells and were both higher in CA3 than in CA1. Furthermore, theoretical models of auto-associative networks predict that more precise tuning curves should correspond to higher stability of the stored set of states.[7,8,14,15] Thus, we uncovered a non-trivial dissociation between long-term tuning stability and tuning precision, implying that distinct neuronal mechanisms control these two seemingly related aspects of the hippocampal spatial code. In addition, short-term stability was dissociated from long-term stability, possibly because of the more dominant effect of variability in neuronal responses when comparing temporally adjacent recordings. Together, our results suggest that a collective assembly organization of hippocampal CA3 place cells contributes to the stable storage of information and its retrieval from long-term memory. Future studies that successfully perturb the recurrent synaptic connectivity within CA3 without directly affecting its inputs or outputs could potentially establish a causal link between the recurrent connectivity and the observed collective assembly organization and long-term stability in this hippocampal subfield.

Other possible sources of the differences between the collective coding properties in CA1 and CA3 could be differences in the inputs they receive from other brain regions. Specifically, the dentate gyrus, a part of the mammalian hippocampal formation, strongly projects to CA3 through its extensive network of mossy fibers.[11,70] Combined with its prominent pattern separation capabilities,[51] the dentate gyrus has been hypothesized to carry well-separated activity patterns onto hippocampal CA3 neurons, supporting the storage of new memories with minimal interference from the traces of older memories already stored in the recurrent connectivity in CA3.[71–74]

The spatial tuning precision and short-term stability in CA3 rapidly reached its mature stage after the first exposure to a novel environment, consistent with the role of CA3 in one-trial contextual learning.[20,32,43,44] In contrast, the spatial tuning in CA1 was less precise and stable in novel environments but significantly refined over the course of familiarization,[32,36] gradually developing spatial tuning properties that are more similar to those in CA3. Considering the extensive input CA1 receives from CA3,[12] our results suggest that CA1 may inherit its tuning properties from CA3 throughout learning, possibly via synaptic plasticity in the Schaffer collateral fibers.[75–77] An alternative mechanism that could underlie the refinement of the spatial code in CA1 is the local reorganization of lateral inhibition; i.e., changes in synaptic strength between CA1 pyramidal cells and interneurons.[57,78–80]

Overall, by imaging from large neuronal populations in the recurrently connected hippocampal CA3, our study provides insights into the neuronal mechanisms that may underlie the formation and maintenance of long-term spatial memories. Our findings help bridge the gap between theoretical models of memory and experimental data by demonstrating how emergent

collective computational capabilities could be implemented in the hippocampal network and contribute to the long-term stability of the neural code.

Limitations of the study

Here, we used the pairwise spatial tuning-curve correlations to study hippocampal emergent assembly organization. While other studies have shown that time-domain population techniques may be powerful in extracting structure from hippocampal recordings,[54,55,58,59,81–83] it is important to make sure that the results obtained from such techniques are not an expected byproduct of simpler features of the data.[84] Specifically, because hippocampal place cells are tuned to position, time-domain population analyses inherently capture the high temporal correlations between place cells that encode the same positions even if they do not exhibit co-activity that is greater than what would be expected based on their individual tuning properties. Solving this issue requires comparing the results against a null hypothesis in which the simpler features (i.e., the tuning of the cells) are maintained but higher-order interactions in the population code are destroyed.[84] We addressed this issue by using the pairwise tuning correlations across directions as a null distribution for uncovering emergent assembly organization of hippocampal place cells. An additional support of an emergent organization that cannot be explained by the tuning of individual cells is our analysis of the noise correlations, which suggested that the temporal co-firing of cells may underlie their higher spatial tuning-curve correlations.

STAR★METHODS

Detailed methods are provided in the online version of this paper and include the following:

SUPPLEMENTAL INFORMATION

Supplemental information can be found online at https://doi.org/10.1016/j.celrep.2023.112119.

ACKNOWLEDGMENTS

Y.Z. is Head of the Mike and Valeria Rosenbloom Center for Positive Neuroscience and is supported by grants from the Belle S. and Irving E. Meller Center for the Biology of Aging, European Research Council (ERC-CoG 101001226), Human Frontier Science Program (RGY0069/2017), and Israel Science Foundation (2113/19). We thank Nachum Ulanovsky, Misha Tsodyks, Ofer Yizhar, Tamir Eliav, David Omer, Shaked Palgi, and Natalie Page for helpful advice and comments on the manuscript.

AUTHOR CONTRIBUTIONS

L.S., A.R., and Y.Z. conceived the project. L.S., N.G., and D.D. conducted the experiments. L.S. analyzed the data. L.S., A.R., and Y.Z. wrote and revised the manuscript with input from D.D. and N.G. Y.Z. and A.R. supervised the research. Y.Z. obtained funding.

DECLARATION OF INTERESTS

The authors declare no competing interests.

Received: September 15, 2022
Revised: November 30, 2022
Accepted: January 30, 2023

REFERENCES

1. Morris, R.G., Garrud, P., Rawlins, J.N., and O'Keefe, J. (1982). Place navigation impaired in rats with hippocampal lesions. Nature *297*, 681–683. https://doi.org/10.1038/297681a0.
2. Maguire, E.A., Gadian, D.G., Johnsrude, I.S., Good, C.D., Ashburner, J., Frackowiak, R.S., and Frith, C.D. (2000). Navigation-related structural change in the hippocampi of taxi drivers. Proc. Natl. Acad. Sci. USA *97*, 4398–4403. https://doi.org/10.1073/pnas.070039597.
3. Scoville, W.B., and Milner, B. (1957). Loss of recent memory after bilateral hippocampal lesions. J. Neurol. Neurosurg. Psychiatry *20*, 11–21. https://doi.org/10.1136/jnnp.20.1.11.
4. O'Keefe, J., and Dostrovsky, J. (1971). The hippocampus as a spatial map: preliminary evidence from unit activity in the freely-moving rat. Brain Res. *34*, 171–175. https://doi.org/10.1016/0006-8993(71)90358-1.
5. O'Keefe, J., and Nadel, L. (1978). The hippocampus as a Cognitive Map (Clarendon Press).
6. Hopfield, J.J. (1982). Neural networks and physical systems with emergent collective computational abilities. Proc. Natl. Acad. Sci. USA *79*, 2554–2558. https://doi.org/10.1073/pnas.79.8.2554.
7. Tsodyks, M. (1999). Attractor network models of spatial maps in hippocampus. Hippocampus *9*, 481–489. https://doi.org/10.1016/j.neuron.2005.10.006.
8. Battaglia, F.P., and Treves, A. (1998). Attractor neural networks storing multiple space representations: a model for hippocampal place fields. Phys. Rev. E *58*, 7738–7753. https://doi.org/10.1103/PhysRevE.58.7738.
9. Treves, A., and Rolls, E.T. (1994). Computational analysis of the role of the hippocampus in memory. Hippocampus *4*, 374–391. https://doi.org/10.1002/hipo.450040319.

10. Marr, D. (1971). Simple memory: a theory for archicortex. Philos. Trans. R. Soc. Lond. B Biol. Sci. *262*, 23–81. https://doi.org/10.1098/RSTB.1971.0078.

11. Amaral, D.G., and Witter, M.P. (1989). The three-dimensional organization of the hippocampal formation: a review of anatomical data. Neuroscience *31*, 571–591. https://doi.org/10.1016/0306-4522(89)90424-7.

12. Ishizuka, N., Weber, J., and Amaral, D.G. (1990). Organization of intrahippocampal projections originating from CA3 pyramidal cells in the rat. J. Comp. Neurol. *295*, 580–623. https://doi.org/10.1002/cne.902950407.

13. Bezaire, M.J., and Soltesz, I. (2013). Quantitative assessment of CA1 local circuits: knowledge base for interneuron-pyramidal cell connectivity. Hippocampus *23*, 751–785. https://doi.org/10.1002/hipo.22141.

14. Tsodyks, M.V., and Feigel'man, M.V. (1988). The enhanced storage capacity in neural networks with low activity level. Europhys. Lett. *6*, 101–105. https://doi.org/10.1209/0295-5075/6/2/002.

15. Palm, G. (2013). Neural associative memories and sparse coding. Neural Network. *37*, 165–171. https://doi.org/10.1016/J.NEUNET.2012.08.013.

16. Lu, L., Igarashi, K.M., Witter, M.P., Moser, E.I., and Moser, M.B. (2015). Topography of place maps along the CA3-to-CA2 axis of the hippocampus. Neuron *87*, 1078–1092. https://doi.org/10.1016/j.neuron.2015.07.007.

17. Mankin, E.A., Sparks, F.T., Slayyeh, B., Sutherland, R.J., Leutgeb, S., and Leutgeb, J.K. (2012). Neuronal code for extended time in the hippocampus. Proc. Natl. Acad. Sci. USA *109*, 19462–19467. https://doi.org/10.1073/pnas.1214107109.

18. Mankin, E.A., Diehl, G.W., Sparks, F.T., Leutgeb, S., and Leutgeb, J.K. (2015). Hippocampal CA2 activity patterns change over time to a larger extent than between spatial contexts. Neuron *85*, 190–201. https://doi.org/10.1016/j.neuron.2014.12.001.

19. Dong, C., Madar, A.D., and Sheffield, M.E.J. (2021). Distinct place cell dynamics in CA1 and CA3 encode experience in new environments. Nat. Commun. *12*, 2977–3013. https://doi.org/10.1038/s41467-021-23260-3.

20. Kemere, C., Carr, M.F., Karlsson, M.P., and Frank, L.M. (2013). Rapid and continuous modulation of hippocampal network state during exploration of new places. PLoS One *8*, e73114. https://doi.org/10.1371/JOURNAL.PONE.0073114.

21. Ziv, Y., Burns, L.D., Cocker, E.D., Hamel, E.O., Ghosh, K.K., Kitch, L.J., El Gamal, A., and Schnitzer, M.J. (2013). Long-term dynamics of CA1 hippocampal place codes. Nat. Neurosci. *16*, 264–266. https://doi.org/10.1038/nn.3329.

22. Ghosh, K.K., Burns, L.D., Cocker, E.D., Nimmerjahn, A., Ziv, Y., Gamal, A.E., and Schnitzer, M.J. (2011). Miniaturized integration of a fluorescence microscope. Nat. Methods *8*, 871–878. https://doi.org/10.1038/nmeth.1694.

23. Chen, T.W., Wardill, T.J., Sun, Y., Pulver, S.R., Renninger, S.L., Baohan, A., Schreiter, E.R., Kerr, R.A., Orger, M.B., Jayaraman, V., et al. (2013). Ultrasensitive fluorescent proteins for imaging neuronal activity. Nature *499*, 295–300. https://doi.org/10.1038/nature12354.

24. Sheintuch, L., Rubin, A., Brande-Eilat, N., Geva, N., Sadeh, N., Pinchasof, O., and Ziv, Y. (2017). Tracking the same neurons across multiple days in Ca2+ imaging data. Cell Rep. *21*, 1102–1115. https://doi.org/10.1016/j.celrep.2017.10.013.

25. Rubin, A., Geva, N., Sheintuch, L., and Ziv, Y. (2015). Hippocampal ensemble dynamics timestamp events in long-term memory. Elife *4*, e12247. https://doi.org/10.7554/eLife.12247.

26. Cai, D.J., Aharoni, D., Shuman, T., Shobe, J., Biane, J., Song, W., Wei, B., Veshkini, M., La-Vu, M., Lou, J., et al. (2016). A shared neural ensemble links distinct contextual memories encoded close in time. Nature *534*, 115–118. https://doi.org/10.1038/nature17955.

27. Kinsky, N.R., Sullivan, D.W., Mau, W., Hasselmo, M.E., and Eichenbaum, H.B. (2018). Hippocampal place fields maintain a coherent and flexible map across long timescales. Curr. Biol. *28*, 3578–3588.e6. https://doi.org/10.1016/J.CUB.2018.09.037.

28. Wagatsuma, A., Okuyama, T., Sun, C., Smith, L.M., Abe, K., and Tonegawa, S. (2018). Locus coeruleus input to hippocampal CA3 drives single-trial learning of a novel context. Proc. Natl. Acad. Sci. USA *115*, E310–E316. https://doi.org/10.1073/pnas.1714082115.

29. Zhou, P., Resendez, S.L., Rodriguez-Romaguera, J., Jimenez, J.C., Neufeld, S.Q., Giovannucci, A., Friedrich, J., Pnevmatikakis, E.A., Stuber, G.D., Hen, R., et al. (2018). Efficient and accurate extraction of in vivo calcium signals from microendoscopic video data. Elife *7*, e28728–e28737. https://doi.org/10.7554/eLife.28728.

30. Leutgeb, S., Leutgeb, J.K., Treves, A., Moser, M.B., and Moser, E.I. (2004). Distinct ensemble codes in hippocampal areas CA3 and CA1. Science *305*, 1295–1298. https://doi.org/10.1126/science.1100265.

31. Mehta, M.R., Quirk, M.C., and Wilson, M.A. (2000). Experience-dependent asymmetric shape of hippocampal receptive fields. Neuron *25*, 707–715. https://doi.org/10.1016/S0896-6273(00)81072-7.

32. Karlsson, M.P., and Frank, L.M. (2008). Network dynamics underlying the formation of sparse, informative representations in the hippocampus. J. Neurosci. *28*, 14271–14281. https://doi.org/10.1523/JNEUROSCI.4261-08.2008.

33. Markus, E.J., Qin, Y.L., Leonard, B., Skaggs, W.E., McNaughton, B.L., and Barnes, C.A. (1995). Interactions between location and task affect the spatial and directional firing of hippocampal neurons. J. Neurosci. *15*, 7079–7094. https://doi.org/10.1523/JNEUROSCI.15-11-07079.1995.

34. Treves, A., and Panzeri, S. (1995). The upward bias in measures of information derived from limited data samples. Neural Comput. *7*, 399–407. https://doi.org/10.1162/neco.1995.7.2.399.

35. Sheintuch, L., Rubin, A., and Ziv, Y. (2022). Bias-free estimation of information content in temporally sparse neuronal activity. PLoS Comput. Biol. *18*, e1009832. https://doi.org/10.1371/JOURNAL.PCBI.1009832.

36. Cacucci, F., Wills, T.J., Lever, C., Giese, K.P., and O'Keefe, J. (2007). Experience-dependent increase in CA1 place cell spatial information, but not spatial reproducibility, is dependent on the autophosphorylation of the α-isoform of the calcium/calmodulin-dependent protein kinase II. J. Neurosci. *27*, 7854–7859. https://doi.org/10.1523/JNEUROSCI.1704-07.2007.

37. Rechavi, Y., Rubin, A., Yizhar, O., and Ziv, Y. (2022). Exercise increases information content and affects long-term stability of hippocampal place codes. Cell Rep. *41*, 111695. https://doi.org/10.1016/j.celrep.2022.111695.

38. Rubin, A., Sheintuch, L., Brande-Eilat, N., Pinchasof, O., Rechavi, Y., Geva, N., and Ziv, Y. (2019). Revealing neural correlates of behavior without behavioral measurements. Nat. Commun. *10*, 4745. https://doi.org/10.1038/s41467-019-12724-2.

39. McNaughton, B.L., Barnes, C.A., and O'Keefe, J. (1983). The contributions of position, direction, and velocity to single unit activity in the hippocampus of freely-moving rats. Exp. Brain Res. *52*, 41–49. https://doi.org/10.1007/BF00237147.

40. Battaglia, F.P., Sutherland, G.R., and McNaughton, B.L. (2004). Local sensory cues and place cell directionality: additional evidence of prospective coding in the hippocampus. J. Neurosci. *24*, 4541–4550. https://doi.org/10.1523/JNEUROSCI.4896-03.2004.

41. Navratilova, Z., Hoang, L.T., Schwindel, C.D., Tatsuno, M., and McNaughton, B.L. (2012). Experience-dependent firing rate remapping generates directional selectivity in hippocampal place cells. Front. Neural Circ. *6*, 6–14. https://doi.org/10.3389/fncir.2012.00006.

42. Law, L.M., Bulkin, D.A., and Smith, D.M. (2016). Slow stabilization of concurrently acquired hippocampal context representations. Hippocampus *26*, 1560–1569. https://doi.org/10.1002/hipo.22656.

43. Nakazawa, K., Sun, L.D., Quirk, M.C., Rondi-Reig, L., Wilson, M.A., and Tonegawa, S. (2003). Hippocampal CA3 NMDA receptors are crucial for memory acquisition of one-time experience. Neuron *38*, 305–315. https://doi.org/10.1016/S0896-6273(03)00165-X.

44. Nakashiba, T., Young, J.Z., McHugh, T.J., Buhl, D.L., and Tonegawa, S. (2008). Transgenic inhibition of synaptic transmission reveals role of CA3

output in hippocampal learning. Science *319*, 1260–1264. https://doi.org/10.1126/science.1151120.

45. Dragoi, G., Harris, K.D., and Buzsáki, G. (2003). Place representation within hippocampal networks is modified by long-term potentiation. Neuron *39*, 843–853. https://doi.org/10.1016/S0896-6273(03)00465-3.
46. Vazdarjanova, A., and Guzowski, J.F. (2004). Differences in hippocampal neuronal population responses to modifications of an environmental context: evidence for distinct, yet complementary, functions of CA3 and CA1 ensembles. J. Neurosci. *24*, 6489–6496. https://doi.org/10.1523/JNEUROSCI.0350-04.2004.
47. Guzowski, J.F., Knierim, J.J., and Moser, E.I. (2004). Ensemble dynamics of hippocampal regions CA3 and CA1. Neuron *44*, 581–584. https://doi.org/10.1016/j.neuron.2004.11.003.
48. Lee, I., Yoganarasimha, D., Rao, G., and Knierim, J.J. (2004). Comparison of population coherence of place cells in hippocampal subfields CA1 and CA3. Nature *430*, 456–459. https://doi.org/10.1038/nature02739.
49. Neunuebel, J.P., and Knierim, J.J. (2014). CA3 retrieves coherent representations from degraded input: direct evidence for CA3 pattern completion and dentate gyrus pattern separation. Neuron *81*, 416–427. https://doi.org/10.1016/j.neuron.2013.11.017.
50. Guzman, S.J., Schlögl, A., Frotscher, M., and Jonas, P. (2016). Synaptic mechanisms of pattern completion in the hippocampal CA3 network. Science *353*, 1117–1123.
51. Leutgeb, J.K., Leutgeb, S., Moser, M.B., and Moser, E.I. (2007). Pattern separation in the dentate gyrus and CA3 of the hippocampus. Science *315*, 961–966. https://doi.org/10.1126/science.1135801.
52. Bakker, A., Kirwan, C.B., Miller, M., and Stark, C.E.L. (2008). Pattern separation in the human hippocampal CA3 and dentate gyrus. Science *319*, 1640–1642. https://doi.org/10.1126/science.1152882.
53. Alme, C.B., Miao, C., Jezek, K., Treves, A., Moser, E.I., and Moser, M.B. (2014). Place cells in the hippocampus: eleven maps for eleven rooms. Proc. Natl. Acad. Sci. USA *111*, 18428–18435. https://doi.org/10.1073/pnas.1421056111.
54. Pfeiffer, B.E., and Foster, D.J. (2015). Autoassociative dynamics in the generation of sequences of hippocampal place cells. Science *349*, 180–183. https://doi.org/10.5061/dryad.gf774.SUPPLEMENTARY.
55. Malvache, A., Reichinnek, S., Villette, V., Haimerl, C., and Cossart, R. (2016). Awake hippocamal reactivations project onto othrogonal neuronal assemblies. Science *353*, 1280–1283. https://doi.org/10.5061/dryad.5gk8j.
56. Harris, K.D., Csicsvari, J., Hirase, H., Dragoi, G., and Buzsáki, G. (2003). Organization of cell assemblies in the hippocampus. Nature *424*, 552–556. https://doi.org/10.1038/nature01765.1.
57. Geiller, T., Sadeh, S., Rolotti, S.V., Blockus, H., Vancura, B., Negrean, A., Murray, A.J., Rózsa, B., Polleux, F., Clopath, C., and Losonczy, A. (2022). Local circuit amplification of spatial selectivity in the hippocampus. Nature *601*, 105–109. https://doi.org/10.1038/s41586-021-04169-9.
58. El-Gaby, M., Reeve, H.M., Lopes-dos-Santos, V., Campo-Urriza, N., Perestenko, P.V., Morley, A., Strickland, L.A.M., Lukács, I.P., Paulsen, O., and Dupret, D. (2021). An emergent neural coactivity code for dynamic memory. Nat. Neurosci. *24*, 694–704. https://doi.org/10.1038/s41593-021-00820-w.
59. Meshulam, L., Gauthier, J.L., Brody, C.D., Tank, D.W., and Bialek, W. (2017). Collective behavior of place and non-place neurons in the hippocampal network. Neuron *96*, 1178–1191.e4. https://doi.org/10.1016/j.neuron.2017.10.027.
60. Posani, L., Cocco, S., Ježek, K., and Monasson, R. (2017). Functional connectivity models for decoding of spatial representations from hippocampal CA1 recordings. J. Comput. Neurosci. *43*, 17–33. https://doi.org/10.1007/s10827-017-0645-9.
61. Hazon, O., Minces, V.H., Tomàs, D.P., Ganguli, S., Schnitzer, M.J., and Jercog, P.E. (2022). Noise correlations in neural ensemble activity limit the accuracy of hippocampal spatial representations. Nat. Commun. *13*, 4276–4313. https://doi.org/10.1038/s41467-022-31254-y.
62. Dragoi, G., and Tonegawa, S. (2014). Selection of preconfigured cell assemblies for representation of novel spatial experiences. Philos. Trans. R. Soc. Lond. B Biol. Sci. *369*, 20120522. https://doi.org/10.1098/rstb.2012.0522.
63. Dragoi, G., and Tonegawa, S. (2011). Preplay of future place cell sequences by hippocampal cellular assemblies. Nature *469*, 397–401. https://doi.org/10.1038/nature09633.
64. Liu, K., Sibille, J., and Dragoi, G. (2019). Preconfigured patterns are the primary driver of offline multi-neuronal sequence replay. Hippocampus *29*, 275–283. https://doi.org/10.1002/hipo.23034.
65. Pastalkova, E., Itskov, V., Amarasingham, A., and Buzsáki, G. (2008). Internally generated cell assembly sequences in the rat hippocampus. Science *321*, 1322–1327. https://doi.org/10.1126/science.1159775.
66. Dragoi, G., and Buzsáki, G. (2006). Temporal encoding of place sequences by hippocampal cell assemblies. Neuron *50*, 145–157. https://doi.org/10.1016/J.NEURON.2006.02.023.
67. Karlsson, M.P., and Frank, L.M. (2009). Awake replay of remote experiences in the hippocampus. Nat. Neurosci. *12*, 913–918. https://doi.org/10.1038/nn.2344.
68. Dragoi, G. (2020). Cell assemblies, sequences and temporal coding in the hippocampus. Curr. Opin. Neurobiol. *64*, 111–118. https://doi.org/10.1016/J.CONB.2020.03.003.
69. Jezek, K., Henriksen, E.J., Treves, A., Moser, E.I., and Moser, M.B. (2011). Theta-paced flickering between place-cell maps in the hippocampus. Nature *478*, 246–249. https://doi.org/10.1038/nature10439.
70. Blackstad, T.W., Brink, K., Hem, J., and Jeune, B. (1970). Distribution of hippocampal mossy fibers in the rat. An experimental study with silver impregnation methods. J. Comp. Neurol. *138*, 433–449. https://doi.org/10.1002/cne.901380404.
71. Treves, A., Tashiro, A., Witter, M.P., and Moser, E.I. (2008). What is the mammalian dentate gyrus good for? Neuroscience *154*, 1155–1172. https://doi.org/10.1016/j.neuroscience.2008.04.073.
72. Acsády, L., and Káli, S. (2007). Models, structure, function: the transformation of cortical signals in the dentate gyrus. Prog. Brain Res. *163*, 577–599. https://doi.org/10.1016/S0079-6123(07)63031-3.
73. Wiskott, L., Rasch, M.J., and Kempermann, G. (2006). A functional hypothesis for adult hippocampal neurogenesis: avoidance of catastrophic interference in the dentate gyrus. Hippocampus *16*, 329–343. https://doi.org/10.1002/hipo.20167.
74. Fiedler, J., De Leonibus, E., and Treves, A. (2021). Has the hippocampus really forgotten about space? Curr. Opin. Neurobiol. *71*, 164–169. https://doi.org/10.1016/j.conb.2021.11.009.
75. Petersen, C.C., Malenka, R.C., Nicoll, R.A., and Hopfield, J.J. (1998). All-or-none potentiation at CA3-CA1 synapses. Proc. Natl. Acad. Sci. USA *95*, 4732–4737. https://doi.org/10.1073/pnas.95.8.4732.
76. Schwartzkroin, P.A., and Wester, K. (1975). Long-lasting facilitation of a synaptic potential following tetanization in the in vitro hippocampal slice. Brain Res. *89*, 107–119. https://doi.org/10.1016/0006-8993(75)90138-9.
77. Herron, C.E., Lester, R.A., Coan, E.J., and Collingridge, G.L. (1986). Frequency-dependent involvement of NMDA receptors in the hippocampus: a novel synaptic mechanism. Nature *322*, 265–268. https://doi.org/10.1038/322265a0.
78. McKenzie, S., Huszár, R., English, D.F., Kim, K., Christensen, F., Yoon, E., and Buzsáki, G. (2021). Preexisting hippocampal network dynamics constrain optogenetically induced place fields. Neuron *109*, 1040–1054.e7. https://doi.org/10.1016/j.neuron.2021.01.011.
79. Grienberger, C., Milstein, A.D., Bittner, K.C., Romani, S., and Magee, J.C. (2017). Inhibitory suppression of heterogeneously tuned excitation enhances spatial coding in CA1 place cells. Nat. Neurosci. *20*, 417–426. https://doi.org/10.1038/nn.4486.

80. Rolotti, S.V., Ahmed, M.S., Szoboszlay, M., Geiller, T., Negrean, A., Blockus, H., Gonzalez, K.C., Sparks, F.T., Solis Canales, A.S., Tuttman, A.L., et al. (2022). Local feedback inhibition tightly controls rapid formation of hippocampal place fields. Neuron *110*, 783–794.e6. https://doi.org/10.1016/j.neuron.2021.12.003.

81. Peyrache, A., Khamassi, M., Benchenane, K., Wiener, S.I., and Battaglia, F.P. (2009). Replay of rule-learning related neural patterns in the prefrontal cortex during sleep. Nat. Neurosci. *12*, 919–926. https://doi.org/10.1038/nn.2337.

82. Gonzalez, W.G., Zhang, H., Harutyunyan, A., and Lois, C. (2019). Persistence of neuronal representations through time and damage in the hippocampus. Science *365*, 821–825. https://doi.org/10.1126/science.aav9199.

83. van de Ven, G.M., Trouche, S., McNamara, C.G., Allen, K., and Dupret, D. (2016). Hippocampal offline reactivation consolidates recently formed cell assembly patterns during sharp wave-ripples. Neuron *92*, 968–974. https://doi.org/10.1016/j.neuron.2016.10.020.

84. Elsayed, G.F., and Cunningham, J.P. (2017). Structure in neural population recordings: an expected byproduct of simpler phenomena? Nat. Neurosci. *20*, 1310–1318. https://doi.org/10.1038/nn.4617.

85. Barretto, R.P.J., Ko, T.H., Jung, J.C., Wang, T.J., Capps, G., Waters, A.C., Ziv, Y., Attardo, A., Recht, L., and Schnitzer, M.J. (2011). Time-lapse imaging of disease progression in deep brain areas using fluorescence microendoscopy. Nat. Med. *17*, 223–228. https://doi.org/10.1038/nm.2292.

86. Guo, Z.V., Hires, S.A., Li, N., O'Connor, D.H., Komiyama, T., Ophir, E., Huber, D., Bonardi, C., Morandell, K., Gutnisky, D., et al. (2014). Procedures for behavioral experiments in head-fixed mice. PLoS One *9*, e88678. https://doi.org/10.1371/journal.pone.0088678.

87. Alexander, G.M., Farris, S., Pirone, J.R., Zheng, C., Colgin, L.L., and Dudek, S.M. (2016). Social and novel contexts modify hippocampal CA2 representations of space. Nat. Commun. *7*, 10300–10314. https://doi.org/10.1038/ncomms10300.

88. Pnevmatikakis, E.A., Soudry, D., Gao, Y., Machado, T.A., Merel, J., Pfau, D., Reardon, T., Mu, Y., Lacefield, C., Yang, W., et al. (2016). Simultaneous denoising, deconvolution, and demixing of calcium imaging data. Neuron *89*, 285–299. https://doi.org/10.1016/j.neuron.2015.11.037.

89. Markus, E.J., Barnes, C.A., McNaughton, B.L., Gladden, V.L., and Skaggs, W.E. (1994). Spatial information content and reliability of hippocampal CA1 neurons: effects of visual input. Hippocampus *4*, 410–421. https://doi.org/10.1002/hipo.450040404.

90. Skaggs, W.E., McNaughton, B.L., Gothard, K.M., and Markus, E.J. (1993). An information-theoretic approach to deciphering the hippocampal code. Proc. IEEE, 1030–1037. https://doi.org/10.1109/PROC.1977.10559.

91. Leutgeb, S., Leutgeb, J.K., Barnes, C.A., Moser, E.I., McNaughton, B.L., and Moser, M.B. (2005). Independent codes for spatial and episodic memory in hippocampal neuronal ensembles. Science *309*, 619–623. https://doi.org/10.1126/science.1114037.

92. Sheintuch, L., Geva, N., Baumer, H., Rechavi, Y., Rubin, A., and Ziv, Y. (2020). Multiple maps of the same spatial context can stably coexist in the mouse hippocampus. Curr. Biol. *30*, 1467–1476.e6. https://doi.org/10.1016/j.cub.2020.02.018.

STAR★METHODS

KEY RESOURCES TABLE

REAGENT or RESOURCE	SOURCE	IDENTIFIER
Bacterial and virus strains		
pAAV2/5-CaMKIIα-GCaMP6f	UNC vector core	Cat #5834
Chemicals, peptides, and recombinant proteins		
C&B Metabond	Parkell	S380
Ultraviolet-curing adhesive	Norland Products Inc.	NOA 81
Flow-It ALC	Pentron	Univ. Opaque
Kwik-Cast	World Precision Instruments	KWIK-CAST
anti- PCP4	Sigma-Aldrich	HPA005792
Donkey-anti-rabbit conjugated to Cy3	Jackson Immuno Research	RRID: AB_2307443
Fluoroshield™ with DAPI	Sigma-Aldrich	F6057
Cy5-Donkey anti-rat	Jackson Immuno Research	RRID: AB_2340672
Deposited data		
Data to produce figures	This paper	https://doi.org/10.5281/zenodo.7523404
Experimental models: Organisms/strains		
C57BL/6J	Envigo Israel	RRID:IMSR_JAX:000,664
Software and algorithms		
Original code	This paper	https://doi.org/10.5281/zenodo.7523404
nVista Acquisition Software	Inscopix inc.	Version 2.0
IC Capture	The imaging source	Version 2.3
MATLAB (version 2014a and onward)	mathworks	https://se.mathworks.com/products/matlab.html
Mosaic	Inscopix inc.	1.1.1b
CNMF-e	(Zhou et al., 2018)[29]	https://github.com/zhoupc/CNMF_E
Unbiased information estimation	(Sheintuch et al., 2022)[35]	https://github.com/zivlab/unbiased_information_estimation
CellReg – cell registration method	(Sheintuch et al., 2017)[24]	https://github.com/zivlab/CellReg
Other		
Integrated miniature fluorescence microscope	Inscopix inc.	nVista 2.0
Gradient refractive index (GRIN) lens	Inscopix inc.	Cat # 1050-002176
Overhead camera for recording animal behavior	The imaging source	DFK 33G445

RESOURCE AVAILABILITY

Lead contact

Further information and requests for resources and reagents should be directed to the lead contact, Yaniv Ziv (yaniv.ziv@weizmann.ac.il).

Materials availability

This study did not generate new reagents.

Data and code availability

- Data to reproduce the figures have been deposited at Zenodo and are available as of the date of publication at https://github.com/zivlab/cell_assemblies. DOI is listed in the key resources table.
- All original code has been deposited at Zenodo and is publicly available as of the date of publication at https://github.com/zivlab/cell_assemblies. DOIs are listed in the key resources table.
- Any additional information required to reanalyze the data reported in this paper is available from the lead contact upon request.

EXPERIMENTAL MODEL AND SUBJECT DETAILS

Animals

All procedures were approved by the Weizmann Institute's IACUC. A total of nine C57BL/6 male mice, aged 5-7 months at the start of the imaging (8-12 weeks at the start of viral injections), were used in this study. Four mice were imaged in hippocampal CA1 and five mice were imaged in hippocampal CA3. Mice were housed with a running wheel in a 12:12 h reverse light cycle.

METHOD DETAILS

Surgical procedures

We used established protocols for *in-vivo* microendoscopy, which allows chronic imaging without any apparent degradation of the imaging quality.[85] We first injected into the CA1 or CA3, under isoflurane anesthesia (1.5-2% volume), 450 nL of viral vector AAV2/5-CaMKIIa-GCaMP6f ($\sim$2X10^{13} particles per ml, packed by University of North Carolina Vector Core)[23] at stereotatic coordinates: $-$1.9 mm anteroposterior, $-$1.4 mm mediolateral, $-$1.6 mm dorsoventral from bregma for CA1, and -1.8 mm anteroposterior, $-$2.1 mm mediolateral, $-$2.05 mm dorsoventral from bregma for CA3. We found in previous work[21,25] that this method yields a stable expression of the GCaMP protein. Mice were then allowed to recover for at least two weeks. Then, we implanted in the CA1 mice a glass guide tube directly above the hippocampus. We used a trephine drill to remove a circular part of the skull. The center of the craniotomy (and accordingly the implanted guide tube) was $\sim$0.25 mm lateral and 0.25 mm posterior to the injection site. We removed the dura and cortex above the CA1 by suction with a 29-gauge blunt needle while constantly washing the exposed tissue with sterile phosphate-buffered saline (PBS). We then implanted the optical guide tube with its window just dorsal to, but not within, the CA1 area and sealed the space between the skull and the guide tube using 1.5% agarose in PBS. The exposed skull areas were then sealed with Metabond (Parkell, Edgewood, NY) and dental acrylic. To optically access hippocampal CA3 without damaging CA1, we implanted a microendoscope equipped with a micro-prism (1 mm diameter, 4 mm length; see Figure 1A). The craniotomy was centered anterolateral to the viral injection site ($-$1.1 mm anteroposterior, $-$2.15 mm mediolateral). Then, after removing the dura and cortex above the hippocampus, we inserted the microendoscope using a stereotax so that the posterolateral edge of the prism was located $-$1.7 mm anteroposterior, $-$2.55 mm mediolateral, $-$2.45 mm dorsoventral from bregma and sealed the space between the skull and the microendoscope with silicon sealant (Kwik-Sil, WPI). Similar to the surgery in CA1, the exposed areas of the skull were then sealed with Metabond (Parkell, Edgewood, NY) and dental acrylic. The microendoscope was sealed with silicon sealant (Kwik-Cast, WPI) for protection until the attachment of a base plate. To perform time-lapse one-photon Ca^{2+} imaging in freely behaving mice using an integrated miniature fluorescence microscope (nVistaHD, Inscopix), we followed a previously established protocol.[21] At least three weeks after guide-tube or micro-prism implantation, mice were imaged under isoflurane anesthesia using a two-photon microscope (Ultima IV, Bruker, Germany). For CA1 mice, we inserted a microendoscope consisting of a single gradient refractive index lens (1 mm diameter, Inscopix) into the guide tube and examined Ca^{2+} indicator expression and tissue health. In both CA1 and CA3 mice, we selected for further imaging only mice that exhibited homogeneous GCaMP6f expression and appeared to have healthy tissue. Mice with clear signs of tissue compression or patches with missing cells were excluded from the study. We also assessed whether there are signs of over-expression, such as nuclear filling of the indicator. Mice in which more than 5% of the cells displayed nuclear expression of the indicator were also excluded from the study. The selected mice were water-restricted until the end of the experiment, and underwent a daily health inspection[86] while ensuring their body weight was above 80% of their initial weight. Water-restriction started a few days prior to attaching the microscope's base plate to avoid changes in the imaging focal plane that may occur during the experiment due to changes in the mice's weight. For the CA1 mice, the microendoscope was then affixed within the guide tube using an ultraviolet-curing adhesive (Norland, NOA81, Edmund Optics, Barrington, NJ). Finally, in both the CA1 and CA3 mice, the microscope's base plate was attached to the dental acrylic cap using a light-cured adhesive (Flow-It ALC, Pentron, Orange, CA).

Ca^{2+} imaging and experimental timeline

A few days after attaching the microscope's base plate, mice were habituated to human handling by allowing them to walk on experimenters' hands. We then began training the water-restricted mice to run back and forth on an elevated, short (56 cm long) linear track with high walls (30 cm high) that was located in a square enclosure within the recording room. Before beginning the Ca^{2+} imaging, we pre-trained the mice for 3 days to run on the short linear track while carrying the head-mounted microscope. Then, we began imaging in a novel straight linear track (environment A, 96 cm long) with low walls (4 cm high). Each imaging day consisted of two 10-min sessions separated by 5 min, during which the mice were placed in a transparent bucket on top of the linear track. Imaging was performed every other day, reaching a total of eight imaging days spanning two weeks. After eight imaging days in the straight linear track, eight additional imaging days were performed every other day in an L-shaped linear track (Environment B, 96 cm long). Three out of the nine mice explored the environments in the opposite order. The environments differed in their geometry and had distinct sets of visual and tactile cues, overhead lights, and odor cues. Before the beginning of each imaging session, we wiped the tracks with differently scented paper towels (10% ethanol for environment A and 0.5% acetic acid for environment B). We trained the mice to run back and forth along the track by giving them a measured amount of water sweetened with 4% sucrose. The water reward was dispensed at both ends of the tracks using a custom-made computer-controlled device. To record mouse behavior, we used an overhead camera (DFK 33G445, The Imaging Source, Germany), which we synchronized with the integrated

microscope. Ca^{2+} imaging was performed 11-18 weeks after viral injection at 10 Hz (N = 1 mouse) or 20 Hz (N = 8 mice), with a spatial downsampling of a factor of four in each dimension (pixel size of 2.3 × 2.3 μm).

Immunohistochemistry

To verify the location of imaging for mice implanted with a micro-prism anterior to CA3, we used PCP4 for the labeling of CA2 neurons[87] (Figure S1A). Mice were transcardially perfused with 4% (wt/vol) paraformaldehyde (PFA) in PBS. The brains were then post-fixed by the same solution for at least 24 h. To stain for PCP4, freely floating sections were incubated with 3% (vol/vol) goat serum in 0.3% (vol/vol) Triton X-100 in PBS for 1 h at room temperature. Sections were then incubated with the primary antibody (rabbit antibody to PCP4, 1:200, HPA005792, Sigma-Aldrich) in 3% goat serum in 0.3% PBS overnight at 4°C. After rinsing three times with PBS, sections were incubated with secondary antibodies (donkey-anti-rabbit conjugated to Cy3, 1:200, 711-165-152, Jackson ImmunoResearch) in PBS with 3% goat serum for 2 h at room temperature. Sections were then mounted on glass slides and covered with mounting medium containing DAPI (F6057, Sigma-Aldrich). Mice in which CA2 was closely aligned with the central part of the micro-prism's location and not with its periphery were excluded from the study.

QUANTIFICATION AND STATISTICAL ANALYSIS

Mouse position tracking

We analyzed mouse behavior videos using a custom MATLAB (Mathworks) routine that detects the mouse's center of mass in each frame. We then used the estimated position to calculate its velocity and applied a smoothing filter (rectangular window of 250 msec) to the calculated velocity.

Processing Ca^{2+} imaging data

We pre-processed the Ca^{2+} imaging data using commercial software (Mosaic, version 1.1.1b, Inscopix) and custom MATLAB routines.[21,25] To correct for lateral displacements of the brain, we used a rigid-body registration. This procedure was performed on a high-contrast sub-region of the movies in which the blood vessels were most prominent. To enhance the appearance of the blood vessels that were used as stationary fiducial markers for image registration, we divided each pixel by the corresponding value from a smoothed image. The smoothed image was obtained by applying a Gaussian filter with a radius of 100 μm to the movies. Ca^{2+} dynamics were then extracted from the registered movies using CNMF-e,[29] an extension of the constrained non-negative matrix factorization method,[88] for one-photon microendoscopic data. This method detects cells in Ca^{2+} imaging data by modeling the videos as a superposition of all neurons' spatiotemporal activity, plus time-varying background and additive noise. The noise components can compensate for spatial and temporal non-uniform illumination in the Ca^{2+} imaging data. The activity of each neuron is expressed as the outer product of a spatial vector, which represents its spatial footprint, and a temporal vector, which represents its Ca^{2+} trace. In addition, by deconvolving the Ca^{2+} trace using an autoregressive model, the method estimates the underlying spiking activity. We used the estimated underlying spike trains as a proxy for the firing rates of the cells. For each mouse, the same parameters ($3 \leq$ gsig ≤ 4; gsiz = 8; $0.7 \leq$ min_corr ≤ 0.85; $8 \leq$ min_pnr ≤ 18) were maintained across all imaging days. CNMF-e allowed the detection of hundreds of neurons per imaging day, and yielded the estimated spike train for each neuron.

Tracking the same neurons across days

To identify the same neurons across multiple imaging days, we used a probabilistic method for cell registration,[24] which estimates the probability of correct registration for each cell in the dataset and the overall rates of registration errors. First, the different days are aligned to one another by maximizing the cross-correlation of the cells' centroid locations between each day and a reference day (day 1). Then, the distribution of Pearson correlations between the spatial footprints (spatial correlation) of pairs of neighboring cells (maximal distance = 14 μm) across days is computed. Next, the distribution of spatial correlation is modeled as a weighted sum of two subpopulations, one corresponding to the same cells and the other to different cells. This allows the estimation of the overall rates of false-positive errors (different cells falsely registered as the same cells) and false-negative errors (the same cells falsely registered as different cells) as a function of the registration threshold ($P_{same} = 0.5$ was used for all mice), allowing a registration that is optimized to the dataset of each mouse. Here, we used the average across the false positive and false negative rates as a measure of registration accuracy. Finally, the obtained P_{same} were used as an input for a clustering algorithm that registered the cells across all imaging days.

Analysis of neuronal spatial tuning

For tuning-curve analysis, we focused on periods when the mouse ran >1 cm/s, while separately considering tuning curves for left and right running directions. We divided each track into 24 bins (4 cm each) and excluded the last 2 bins at both ends of the tracks where water rewards are consumed and the mice are generally stationary.[21] We then computed the time spent in each bin in each running direction, and the number of spikes per bin. Finally, we computed the tuning curve for each neuron by dividing the spike number in each bin by the time spent in that bin. The preferred position of each place cell was defined as the bin with the highest value.

Estimating spatial information and identifying place cells

For each cell with $\geq$10 active time bins in a given day, we first applied the naive estimation of spatial information content (in bit per spike):[89]

$$spatial\ information = \sum_i p_i(r_i/\bar{r})log_2(r_i/\bar{r}),$$

where r_i is the estimated firing rate of the neuron in the i^{th} bin, p_i is the probability of the mouse being in the i^{th} bin (time spent in i^{th} bin/total session time), $\bar{r}$ is the overall mean estimated firing rate, with i running over all the bins. We then performed 1,000 distinct cyclic shuffles, and calculated the spatial information for each shuffle.[90] This yielded the p value of the measured information relative to the shuffles. Cells with $p < 0.05$ were considered significant place cells and used for further analysis. To correct for the upward bias in the naive estimation of spatial information from limited sample sizes,[34] we used two recently developed methods that are specifically tailored for the temporally sparse neuronal activity extracted from Ca^{2+} imaging data.[35] The first method assumes a fixed ratio between the bias in the shuffle information (i.e., the deviation of the shuffle from zero) and the bias in naive estimation. Based on this assumption, a scaled version of the shuffle information is subtracted from the naive estimation for each cell. The second method is based on fitting a curve to the naive estimation as a function of the sample size and extrapolating the fitted curve to infinite sample sizes. We also verified that both methods yielded similar estimated information. The results presented in the figures are according to the scaled shuffle reduction method.

Number of place fields and field size

To estimate the number of place fields and the field size for each place cell, we binarized the tuning curves, setting all values that are > 30% of the maximal value to 1 and the rest to 0. Then, we counted the number of separate place fields in the binarized tuning curves (done for each running direction separately). The size of the place field was defined as the size of the field surrounding the maximal value of the tuning curve, i.e., the most dominant field.

Population vector correlation

To determine the level of similarity between representations of the environment on different sessions, we calculated the mean population vector (PV) correlation (Pearson correlation) between them.[91] For each spatial bin (excluding the last 2 bins at each end of the tracks, and separating between right and left running directions), we defined the PV as the mean estimated spike rate for each neuron given that bin's occupancy. We computed the correlation between the PV in one session with that of the matching position in another session, and averaged the correlations over all positions. For each pairwise comparison, we used only cells that passed the place cell significance test in at least one of the two sessions. Since in some cases the hippocampus can switch between multiple orthogonal maps (global remapping) across sessions in the same environment,[92] we separated between the different maps observed in each environment and considered only within-map PV correlations. Each session that had at least one session from another day with which it had a PV correlation > 0.1 was identified to belong to that specific map, resulting in an unambiguous separation of the different sessions into the different maps. Overall, we found 4/64 occurrences in CA1 and 3/80 occurrences in CA3 of a switch to a map other than the one displayed in most of the days. We also used PV correlations to quantify the similarity of the spatial code across the two running directions. Since previous work found that place fields are displaced across the two directions in a linear track,[40] we defined the between-directions PV correlations as the one obtained for the displacement value that maximizes the correlation.

Tuning-curve correlation

For each place cell, we determined the level of similarity between the representations of the environment on different sessions by calculating the tuning curve correlation (Pearson correlation) between the two sessions (done for each running direction separately). Cells that were significantly spatially tuned in at least one of the two sessions were considered to be place cells. As done for the PV correlations, we separated between the different maps observed in each environment and considered only within-map tuning correlations.

Ensemble rate correlation

To quantify the similarities in activity patterns between sessions, without accounting for place tuning, we measured the overall estimated spike rate for each neuron in each session (irrespective of mouse position). We then calculated the ensemble rate correlation (Pearson correlation) between the vectors (for all neurons) of estimated spike rates. As done for the PV correlations, we separated between the different maps observed in each environment and considered only within-map ensemble rate correlations.

Organization into assemblies of correlated place cells

To analyze the structure of pairwise correlations in the neuronal population, we measured the tuning-curve correlations (Pearson correlation) between all pairs of place cells in a given session. To test whether or not the spatial tuning curves of hippocampal place cells were organized into assemblies of correlated cells, we focused on pairs of cells with the same preferred positions and calculated the distribution of their tuning-curve correlations. Then, for each mouse, we compared this distribution against the distribution obtained

in the same mouse for pairs of cells with the same preferred position across the opposite running directions in the linear track. This procedure controlled for the differences in tuning precision and average estimated firing rates between individual mice and between the two hippocampal subfields. As an additional validation, we compared the within-mouse distribution of tuning correlations against the distribution obtained across cells with the same preferred position that were imaged from different mice in the same hippocampal subfield. This validation also controlled for possible non-idiosyncratic overrepresentations of specific locations within the environment. We also compared the distributions of pairwise tuning-curve correlations for cells with different preferred positions.

Tuning peer-dependence

We quantified for each place cell the dependence of its tuning on the tuning of other place cells. To calculate the tuning peer-dependence of a given cell, we found the median of its within-direction pairwise tuning correlations and then calculated in what percentile it falls within the distribution of its across-directions tuning correlations. To test the relationship between tuning stability, precision, and peer-dependence, we separately fitted to the data of each hippocampal subfield a linear multiple regression model between the tuning-curve correlation, spatial information, tuning peer-dependence, average estimated firing rate, and mouse identity of each cell. Next, we divided the population into the cells with a median pairwise tuning correlation > 95 percentile of the across-directions distribution (peer-dependent cells) and the cells with lower percentiles (peer-independent cells). Finally, we compared the different properties of the neural code across these groups of cells. Since the PV correlation is a measure that is sensitive to population size, a subset of peer-independent cells was randomly chosen for each pair of sessions to match the peer-dependent cells' population size.

Distribution of preferred positions

To test for differences in the distributions of preferred positions between peer-dependent and peer-independent cells, we compared the degree to which these distributions diverged from a uniform distribution. This analysis was performed using the Kullback–Leibler divergence (D_{KL}):

$$D_{KL} = -\sum_i p_i^{data} log_2\left(p_i^{uniform} / p_i^{data}\right),$$

where p_i^{data} is the fraction of cells with a preferred position in the i^{th} bin, and $p_i^{uniform}$ is the fraction based on a uniform distribution, i.e., 1 over the number of spatial bins. The distributions of preferred positions and D_{KL} were estimated separately for each environment and running direction and the obtained values were averaged across environments and directions for each mouse.

Pairwise noise correlations

Noise correlations were calculated by first measuring the temporal correlations (Pearson correlation) between the estimated spike trains of pairs of neurons for a given mouse position. Then, for each pair of cells, we calculated the weighted average of these correlations over all positions along the track, where the weights were the probability of the mouse to be in a given position. This yielded a single value representing the average noise correlation for each pair of cells. Finally, we calculated the noise correlations as a function of the difference between the preferred positions of pairs of place cells and as a function of the distance between the locations of the cells in the brain tissue.

Statistical analysis

For unrelated samples from two different groups, we performed a Mann-Whitney U-test. For matched-pairs related samples, we performed a two-sided matched-pairs t test. For repeated measurements from one group, we performed one-way repeated-measures ANOVA. For repeated measurements from unrelated samples from two different groups, we performed two-way repeated-measures ANOVA. For repeated measurements of matched-pairs related samples, we used Friedman's test, a non-parametric test similar to repeated-measures ANOVA. The relationship between tuning stability, tuning precision, and tuning peer-dependence was tested using a linear multiple regression analysis.